



RESEARCH ARTICLE

PHOTOCATALYTIC DEGRADATION OF METHYLENE BLUE AND BRILLIANT GREEN USING TiO₂,
LOADED ON GROUNDNUT SHELL ACTIVATED CARBON UNDER SUNLIGHT RADIATION

Ragupathy, S. and *Raghu, K.

Department of Physics, Annamalai University, Annamalai Nagar, Chidambaram- 608 002, Tamilnadu, India

ARTICLE INFO

Article History:

Received 21st June, 2014
Received in revised form
16th July, 2014
Accepted 19th August, 2014
Published online 18th September, 2014

Key words:

TiO₂, TiO₂/GNSAC, Dyes,
Adsorption Kinetic,
Photocatalysis, Sunlight.

ABSTRACT

Titanium dioxide and Titanium dioxide loaded groundnut shell activated carbon photocatalytic activity were synthesized by sol-gel technique. The preparation of TiO₂ and TiO₂/GNSAC photocatalysts were achieved by titanium tetra isopropoxide and 2-propanol as common starting materials and annealed the product at 500 °C for 2 h to get anatase phase, respectively. The prepared materials were characterized by X-ray diffraction analysis (XRD), Fourier transform infrared spectroscopy (FT-IR), and UV-Vis-diffuse reflectance spectroscopy (DRS). The photocatalytic activity was tested and compared with that of TiO₂ and TiO₂/GNSAC on the degradation of methylene blue (MB) and brilliant green (BG) in an aqueous solutions using sunlight radiation. The adsorption kinetics followed both the pseudo-first-order and second-order giving a better fit. The TiO₂/GNSAC removal over 95.39% of BG and 81.57% of MB dyes and its adsorption was fitted best to all models.

Copyright © 2014 Ragupathy, S. and Raghu, K. This is an open access article distributed under the Creative Commons Attribution License, which permits unrestricted use, distribution, and reproduction in any medium, provided the original work is properly cited.

INTRODUCTION

Now-a-days, organic dyes are the major groups of pollutants found in waste waters produced from different industries. It is estimated that around 700,000 tons of dyes are produced annually around the world. From this amount about 20% is unloaded as industrial wastes without previous treatment (Carneiro *et al.*, 2007). Synthetic dyes are commonly used in several manufacturing industries such as textile dyeing, paper printing, cosmetics and pharmaceuticals, and it is estimated that 10 – 15% of the dyestuff lost in the effluent during the dyeing processes (Sayan and Edecan 2008). Removal of environmental pollutants through semiconductor photocatalysis has attracted extensive interest over the last few decades. Among various semiconductors, TiO₂ has been known as the leading photocatalyst due to its good photoactivity, high chemical stability, low cost, and non-toxicity (Hoffmann *et al.*, 1995). There are many methods to prepare TiO₂ such as, sol-gel (Zhang and Banfield 2005), hydrothermal (Andersson *et al.*, 2002), Chemical vapor deposition (Pradhan *et al.*, 2003), and physical vapor deposition (Xiang *et al.*, 2005). Furthermore, TiO₂ is a wide band-gap semiconductor (3.20 eV for anatase TiO₂ and 3.02 eV for rutile TiO₂) which makes the photocatalytic activity quite limited in the visible light, solar and fluorescent light (Ibrahim and Lasa 2002). Recently, an intense effort has been devoted to loading TiO₂ on different supports such as TiO₂/SiO₂, TiO₂/Zeolite, and TiO₂/AC. TiO₂

supports activated carbon which is the porous material and increases its adsorption capacity of organic compounds (Shankar *et al.*, 2006; Maruga *et al.*, 2006; Zhang *et al.*, 2005; Yazawa *et al.*, 2009; Yu *et al.*, 2005). It has been reported that TiO₂ supported on activated carbon has synergistic effect based on the adsorption capacity of activated carbon and the photoactivity of TiO₂ (Wang *et al.*, 2009). Activated carbon (AC) has been suggested as an effective support for TiO₂ in the removal of the pollutants (Deng *et al.*, 2002; Nazir *et al.*, 2003). The present study is encompasses synthesis of TiO₂ and TiO₂/GNSAC by a sol-gel process and their characterization via different techniques such as XRD, UV-Vis (DRS), and FT-IR. Brilliant green and methylene blue are selected to evaluate the photocatalytic activity of TiO₂ and TiO₂/GNSAC catalysts in the sunlight radiation. The kinetic and equilibrium data were analyzed and different models are applied to fit the experimental data.

MATERIALS AND METHODS

Preparation of TiO₂ and loaded GNSAC

The groundnut shell activated carbon (GNSAC) and titanium dioxide (TiO₂) was synthesized by sol-gel method at room temperature. Initially TiO₂ was prepared directly by titanium tetra isopropoxide (C₁₂H₂₈O₄Ti assay ≥ 98%) and 2-propanol (C₃H₈O assay > 99%). 10 mL of titanium tetra isopropoxide was dissolved in 90 mL of 2-propanol to obtain TiO₂. After stirring for 5 min at room temperature, 30 mL of water was added drop wise with vigorous magnetic stirring to obtain

*Corresponding author: Raghu, K.

Department of Physics, Annamalai University, Annamalai Nagar,
Chidambaram- 608 002, Tamilnadu, India.

TiO_2 . The solution was maintained by stirring for 2 h until a homogenous gel was formed. The $\text{TiO}_2/\text{GNSAC}$ catalyst was prepared by a similar method by adding 2.8 g of GNSAC (50 wt% with regard to the TiO_2 amount) to the titanium tetra isopropoxide 2-propanol solution. After stirring the solution was filtered by using whatman filter paper (11 mm) and washed several times using ethanol and deionized water. The precipitate formed was dried at 100 °C for 5 h to evaporate water and organic residue. Then the dried powders were ground using an agate mortar to avoid agglomeration. Finally the powders were kept in muffle furnace and calcinated at 500 °C for 2 h to obtain TiO_2 and $\text{TiO}_2/\text{GNSAC}$ samples.

Characterization

The crystal structures and particle size of GNSAC, TiO_2 and $\text{TiO}_2/\text{GNSAC}$ were analyzed by X-ray diffraction (XRD) measurement which was carried out by using XPERT-PRO diffractometer system using Cu-K α radiation ($\lambda = 1.5406 \text{ \AA}$), as in the 2θ range from 10 to 80°, operating at 30 mA and 40 kV. The functional groups were determined by Fourier transform infrared spectroscopy (FT-IR). Spectra of the samples were recorded using NICOLET AVATAR 330. The samples were scanned 16 times per minute and spectra were recorded in the region 4000–400 cm^{-1} with wave number accuracy of 0.01 cm^{-1} . The diffuse reflectance spectra (DRS) were recorded at wavelength in the range of 300–800 nm by UV-Vis-NIR spectrophotometer (Varian/Carry 5000) equipped with an integrating sphere and the baseline correction was performed using a calibrated reference sample of powdered barium sulfate (BaSO_4).

Photocatalytic experiments

Photocatalytic activities of TiO_2 and loaded GNSAC composite photocatalysis were evaluated by the decolorization of MB and BG dyes aqueous solution under sunlight radiation. The optimum amount of catalysts TiO_2 and $\text{TiO}_2/\text{GNSAC}$ (0.25 and 0.2 g/L respectively) were separately added to 100 mL of MB and BG solutions of initial dyes concentration 10 mg/L. Under magnetic stirring, the mixed solution was irradiated under sunlight. Then solutions were taken out at different times, and centrifuged separation. The concentration of MB and BG in supernatant was analyzed by the absorption intensity at respective maximum absorbance wavelength of MB and BG by using a UV-Vis spectrophotometer (Shimadzu UV1800). Direct sunlight was used in the present study and solar intensity ($1250 \times 100 \text{ Lu} \pm 100$) was almost constant during all the experiments which were conducted between 11.00 a.m. and 2.00 p.m.

The degradation efficiency (%) of MB and BG dyes was calculated from the following equation.

$$\text{Degradation efficiency (\%)} = \frac{C_0 - C_t}{C_0} \times 100 \quad \dots \dots (1)$$

The amount of MB and BG dyes solution adsorbed by TiO_2 and $\text{TiO}_2/\text{GNSAC}$, q_t (mg/g) at each time interval was calculated according to the expression:

$$q_e \left(\frac{\text{mg}}{\text{g}} \right) = \frac{(C_0 - C_t)V}{m} \quad \dots \dots \dots (2)$$

Where C_0 is the initial concentration of MB and BG dyes solution (mg/L) C_t is the concentration of dyes after irradiation in selected time interval (mg/L), V is the volume of the BG and MB dyes solution (mL), and m is the amount of the TiO_2 and $\text{TiO}_2/\text{GNSAC}$ used (g).

RESULTS AND DISCUSSION

Phase and crystallite size analysis

The XRD patterns of the prepared TiO_2 and $\text{TiO}_2/\text{GNSAC}$ composites annealed at 500 °C for 2 h and GNSAC are shown in Fig. 1a-c. Figure 1a the diffraction profile of GNSAC exhibits two broad peaks at $2\theta = 26$ and 43° which are similar to the peaks of crystalline carbonaceous structure and the absence of sharp peak reveals a predominantly amorphous structure. Fig. 1b & c show sharp peaks exhibiting the crystalline nature of TiO_2 and $\text{TiO}_2/\text{GNSAC}$. Average particle size of TiO_2 and $\text{TiO}_2/\text{GNSAC}$ are calculated using the Scherrer formula given by,

$$D = \frac{K\lambda}{\beta \cos\theta} \quad \dots \dots \dots (3)$$

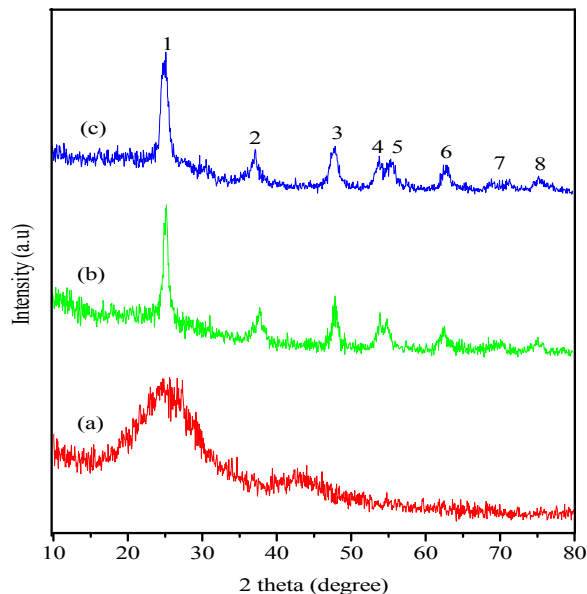
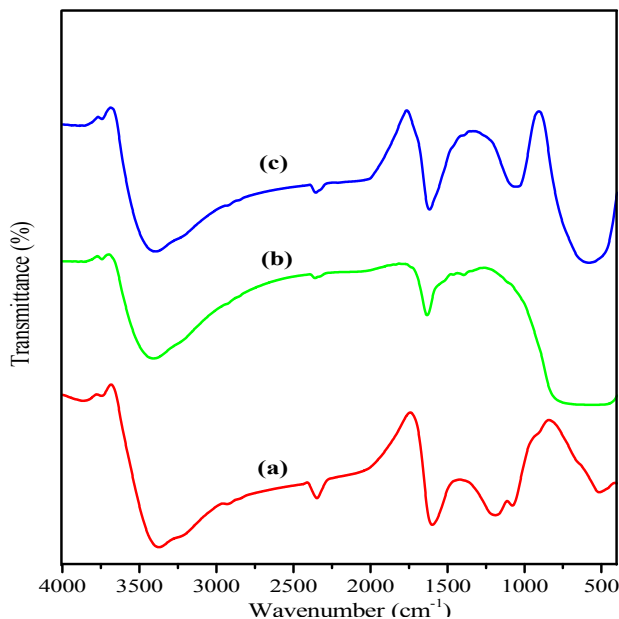
Where D is the average crystallite diameter (nm), K is the Scherrer constant (0.9), λ is the wavelength (1.5406 Å), β is the Full width at half maximum, and θ is the Bragg angle (Slimena *et al.*, 2011). The crystallite sizes corresponding to different 2θ values are compared in Table 1. The average crystallite size of TiO_2 and $\text{TiO}_2/\text{GNSAC}$ are calculated to be 18.79 and 8.7 nm, respectively. The XRD peaks exactly match with the anatase phase of TiO_2 showing that GNSAC modification does not change the phase. The broadening of peaks implies the decrease in crystalline size of TiO_2 and the corresponding increase in porosity of GNSAC favors the adsorption of MB and BG. Besides, well-developed porous structure of GNSAC exposed to TiO_2 , results in increase in number of active sites. Thus, this may contribute to the higher photocatalytic activity of $\text{TiO}_2/\text{GNSAC}$.

Fourier transform infrared spectroscopy

Fig. 2a-c shows the FT-IR spectra of GNSAC and TiO_2 , $\text{TiO}_2/\text{GNSAC}$ nanoparticle after calcination at 500 °C for 2 h. In Fig. 2a for the groundnut shell activated carbon, of the sharp peak located at 2931 cm^{-1} corresponds to aliphatic C-H stretching vibrations in methyl and methylene groups, while the band at 1599 cm^{-1} to C=C stretching of aromatic group (Mahmoodi *et al.*, 2011). The peak at 1188.15 cm^{-1} is assigned to the stretching vibration P-O-C (aromatic) linkage and P=OOH (Hadoun *et al.*, 2013). The broad band at 1300–900 cm^{-1} in GNSAC has a maximum at 1078.21 cm^{-1} . The adsorption in this region is the characteristics for phosphorous. These bands arise as a result of phosphoric acid impregnation during GNSAC synthesis. Spectra of both TiO_2 and $\text{TiO}_2/\text{GNSAC}$ are found to have significant hydroxyl groups on their surface.

Table 1. Comparisons of X-ray diffraction peaks (2 θ °) and average crystallite sizes

	Peaks								Average crystallite size (nm)
	1	2	3	4	5	6	7	8	
TiO ₂	25.34	37.75	47.96	53.82	54.9	62.6	68.7	75.08	18.79
TiO ₂ /GNSAC	25.27	37.82	48	53.85	54.97	62.61	68.76	75.14	8.7
Anatase (JCPDS:71-1166)	25.3 (101)	37.7(004)	48 (200)	53.8(105)	55.0(212)	62.69 (204)	68.75 (116)	75.05 (215)	-

**Figure 1. XRD patterns of (a) GNSAC (b) TiO₂ and (c) TiO₂/GNSAC****Figure 2. FT-IR spectra of (a) GNSAC (b) TiO₂ and (c) TiO₂/GNSAC**

A broad band is observed between 3600 and 3000 cm^{-1} is related to the O-H stretching mode of hydroxyl group, indicating the presence of moisture in the samples. The characteristic peak at 1633 cm^{-1} is associated with the O-H bending vibrations of the adsorbed water molecules. The two observed peaks at 3412 and 1633 cm^{-1} correspond to the surface adsorbed water and hydroxyl groups (Kathiravan and Renganathan 2009) and the presence of OH bands in the spectrum is owing to chemically and physically adsorbed H₂O on the surface of nanoparticle (Olurode *et al.*, 2012). A new peak at 1064 cm^{-1} can be assigned to C-O stretching vibration. For the pure TiO₂, the broad peak at range from 800-400 cm^{-1} is the contributions from the anatase titania. A broad absorption band between 800 and 450 cm^{-1} region is ascribed to the vibration absorption of the Ti-O-Ti linkages in TiO₂/GNSAC (Lu *et al.*, 2008). Thus, TiO₂ particles are proved to be well-distributed on the surface of GNSAC. The FT-IR results, strongly confirm the presence of hydroxyl groups in the structure of the TiO₂/GNSAC.

UV-Vis diffuse reflectance spectroscopy

The diffuse reflectance spectra of TiO₂ and loaded GNSAC photocatalytic are illustrated in Fig. 3 in the 300-800 nm wavelength range. The TiO₂ showed an intense absorption in UV region and the absorption edge of titania can be easily discerned. Compared with bulk TiO₂ (Ravichandran *et al.*, 2009), a shift of the reflectance spectrum of nano-TiO₂ towards the lower wavelength region was observed. The band gap energies (E_g) of TiO₂ and loaded GNSAC are obtained from the wavelength value corresponding to the intersection point of the vertical and horizontal part of the spectrum, using the equation (Zhao *et al.*, 2010):

$$E_g = \frac{hc}{\lambda} \text{ eV}; E_g = \frac{1240}{\lambda} \text{ eV} \quad (4)$$

Where E_g is the band gap energy (eV), h is the Planck's constant (6.626×10^{-34} Js), c is the light velocity (3×10^8 m/s) and λ is the wavelength (nm). The calculated band gap energies are 3.39 eV and 3.44 eV for TiO₂ and TiO₂ loaded GNSAC, respectively. This figure also exhibits the decrease in reflectance and increase in absorbance in the visible region for TiO₂/GNSAC.

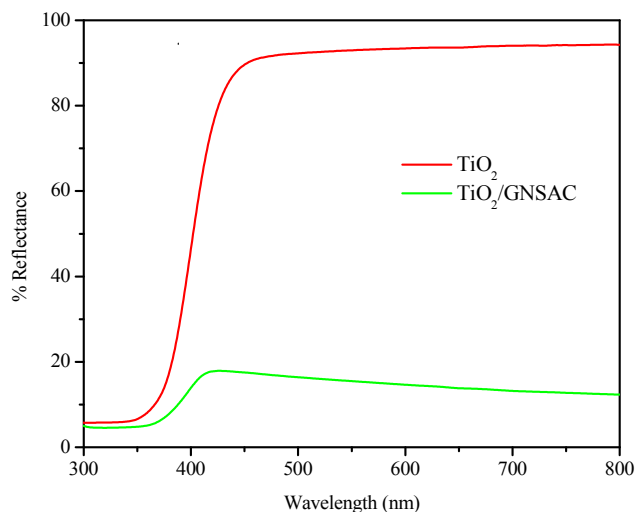


Figure 3. UV-Vis-diffuse reflectance spectra of TiO_2 and $\text{TiO}_2/\text{GNSAC}$

Effect of contact time on Photocatalytic degradation of dyes solution

Photocatalytic experiment was carried out to assess the photocatalytic efficiency of TiO_2 and $\text{TiO}_2/\text{GNSAC}$ on MB and BG at initial dyes concentration of 10 mg/L. Fig. 4a & b show the degradation efficiency of TiO_2 and $\text{TiO}_2/\text{GNSAC}$ on MB and BG, respectively. It can be seen that the increase in the contact time on photodegradation efficiency of naked TiO_2 on MB and BG reached 86.28% and 67.4% respectively, within 120 min irradiation time. However in case of $\text{TiO}_2/\text{GNSAC}$, the highest efficiency reached to 95.39% and 81.57% in the same irradiation time. This fact confirms the higher surface area of the $\text{TiO}_2/\text{GNSAC}$. The result indicates that there is an interaction between $\text{TiO}_2/\text{GNSAC}$ and titania and the size of the $\text{TiO}_2/\text{GNSAC}$ gets smaller and the surface area has increased.

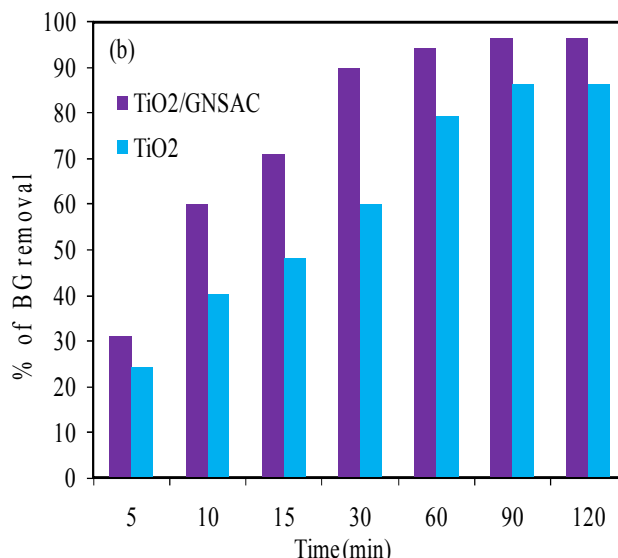
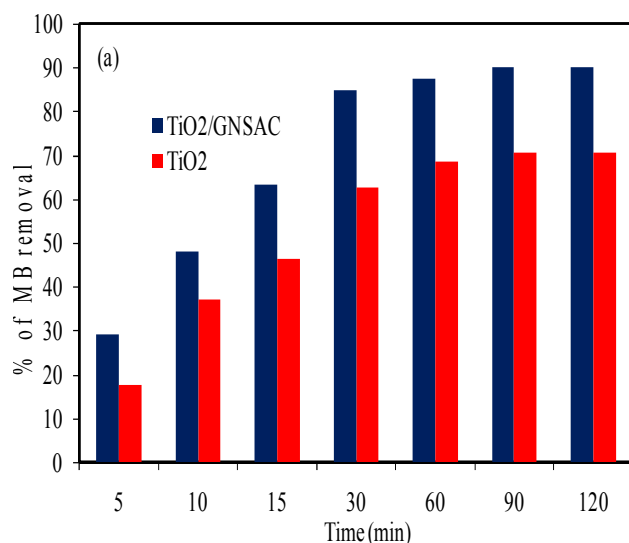


Figure 4. Effect of contact time and photocatalytic degradation of (a) MB and (b) BG removal by composite catalysts TiO_2 and $\text{TiO}_2/\text{GNSAC}$

Mechanism of degradation

The mechanism of photocatalytic oxidation processes has been reported in the literature (Chong *et al.*, 2010; Ahmed *et al.*, 2011). The GNSAC may improve the thermal stability of TiO_2 , the increase in of crystalline size and the surface area and thus preserve a higher content of surface hydroxyl groups (Wang *et al.*, 2009). The $\text{TiO}_2/\text{GNSAC}$ is the most effective due to the synergistic effects of the adsorptive properties of GNSAC and photocatalytic activity of the TiO_2 in the composite. Owing to its high performance ability, the composite $\text{TiO}_2/\text{GNSAC}$ is a very promising photocatalyst for the degradation of organic pollutants.

Adsorption kinetic

Pseudo-second-order model

The pseudo-second-order equation (Mckay and YS 1999), based on equilibrium adsorption, is expressed as,

$$\frac{t}{q_t} = \frac{1}{k_2 q_e^2} + \frac{1}{q_e} t \quad (5)$$

where $h = k_2 q_e^2$, h (mg/g min) is initial adsorption rate and k_2 (g/mg min) is the rate constant of pseudo-second-order adsorption. The value of q_e (mg/g) and k_2 (g/mg min) can be obtained from the slope and the intercept of the t/q_t versus t plots are shown in Fig. 5. The plots being straight lines with correlation coefficient show the applicability of this model for interpretation of experimental. Value of k_2 and q_e are calculated from the intercept and slope of the plots of t/q_t versus t , are shown in Table 2. R^2 value for pseudo-second-order kinetic model is high (0.995) for $\text{TiO}_2/\text{GNSAC}$ and the calculated q_e value is close to the experimental data.

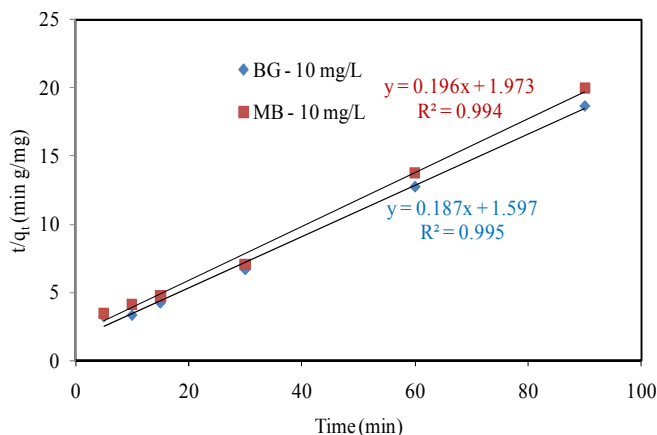


Figure 5. Pseudo-second-order for the adsorption of MB and BG onto TiO₂/GNSAC (catalyst dose = 0.2 g/L)

Table 2. Kinetics parameters for adsorption of pseudo-second-order models for two dyes at 30°C

C ₀ (mg/L)	q _{e, exp} (mg/g)	Pseudo-second-order model			
		k ₂ (g/mg min)	q _{e, cal} (mg/g)	h (mg/g min)	R ²
10-MB	4.511	0.0199	5.076	0.513	0.994
10 -BG	4.821	0.0218	5.347	0.626	0.995

Conclusion

The increase in the photocatalytic activity of TiO₂ by addition of groundnut shell activated carbon was observed. The photocatalytic was characterized by various analytical methods such as XRD, FT-IR, and UV-DRS. The XRD analysis of (101) plane of the anatase phase was clearly observed and its intensity was decreased when compared with that of TiO₂. These results indicated that the anatase TiO₂ particles were well supported on the surface of GNSAC. The FT-IR spectra confirmed the presence of hydroxyl group on TiO₂/GNSAC. Using UV-Vis-DRS analysis, the calculated band gap energies were 3.39 eV and 3.44 eV for TiO₂ and TiO₂ loaded GNSAC. The experiments revealed that the photocatalytic oxidation of MB and BG aqueous solution was more effective in TiO₂ and TiO₂/GNSAC. About 86.28% and 67.4% degradation of BG and MB was observed with TiO₂ and 95.39% and 81.57% degradation of BG and MB was observed with TiO₂/GNSAC using sunlight radiation respectively within 120 min irradiation time. The higher photocatalytic oxidation efficiency of TiO₂/GNSAC at neutral pH was due to higher surface area of GNSAC. An optimum catalyst dose of 0.2 g/L was used throughout the experiments. The photocatalytic reactions appeared to follow pseudo-second-order kinetic model.

REFERENCES

- Ahmed, S., Rasul, M.G., Brown, R., Hashib, M.A. 2011. Influence of parameters on the heterogeneous photocatalytic degradation of pesticides and phenolic contaminants in wastewater: a short review. *J. Environ. Manage.* 92: 311–330.
- Andersson, M., Osterlund, L., Ljungstrom, S., Palmqvist, A. 2002. Preparation of nanosize anatase and rutile TiO₂ by hydrothermal treatment of microemulsions and their activity for photocatalytic wet oxidation of phenol. *J. Phys. Chem. B* 106: 10674–10679.
- Carneiro, P.A., Pupo Nogueira, R.F., Zanoni, M.V.B. 2007. Homogenous photodegradation of C.I. reactive blue 4 using a photo-fenton process under artificial and solar irradiation. *Dye Pigment* 74: 127–132.
- Chong, M.N., Jin, B., Chow, C.W.K., Saint, C. 2010. Recent developments in photocatalytic water treatment technology: a review. *Water Res.* 44: 2997–3027.
- Deng, X., Yue, Y., Gao, Z. 2002. Gas-phase photo-oxidation of organic compounds over nanosized TiO₂ photocatalysts by various preparations. *Appl. Catal. B: Environ.* 39: 135–147.
- Hadoun, H., Sadaoui, Z., Souami, N., Toumert, I. 2013. Characterization of mesoporous carbon prepared from date stems by H₃PO₄ chemical activation. *Appl. surface sci.* 280: 1–7.
- Hoffmann, M.R., Martin, S.T., Choi, W.Y. 1995. Environmental applications of semiconductor photocatalysis. *Chem. Rev.* 95: 69–96.
- Ibrahim, H., Lasa, H. 2002. Photo-catalytic conversion of air borne pollutants, effect of catalyst type and loading in novel photo-CREC-air unit. *Appl. Catal. B: Environ.* 38: 201–213.
- Kathiravan, A., Renganathan, R. 2009. Photosensitization of colloidal TiO₂ nanoparticles with phycocyanin pigment. *J. Colloid Interface Sci.* 335: 196–202.
- Lu, X., Lv, X., Sun, Z., Zheng, Y. 2008. Nanocomposites of poly (L-lactide) and surface-grafted TiO₂ nanoparticles: Synthesis and characterization. *Eur. Polym. J.* 44: 2476–2481.
- Mahmoodi, N.M., Salehi, R., Arami, M. 2011. Binary system dye removal from colored textile wastewater using activated carbon: Kinetic and isotherm studies. *Desalination* 272: 187–195.
- Maruga, J., Hufschmidt, D., Lopez-Munoz, M.J., Selzer, V., Bahnemann, D. 2006. Photonic efficiency for methanol photooxidation and hydroxyl radical generation on silica-supported TiO₂ photocatalysts. *Appl. Catal. B: Environ.* 62: 201–207.
- Mckay, G., YS, H.O. 1999. Pseudo-second-order model for sorption processes. *Bio Chem.* 34: 451–465.
- Nazir, M., Takaski, J., Kumazawa, H. 2003. Photocatalytic degradation of gaseous ammonia and trichloroethylene over TiO₂ ultrafine powders deposited on activated carbon particles. *Chem. Eng. Comm.* 190: 322–333.
- Olurode, K., Neelgund, G.M., Oki, A., Luo, Z. 2012. A facile hydrothermal approach for construction of carbon coating on TiO₂ nanoparticles. *Spectrochim. Acta part A* 89: 333–336.
- Pradhan, S.K., Reucroft, P.J., Yang, F. 2003. Growth of TiO₂ nanorods by metalorganic chemical vapor deposition. *J. Cryst. Growth* 256: 83–88.
- Ravichandran, L., Selvam, K., Krishnakumar, B., Swaminathan, M. 2009. Photovvalorisation of pentafluorobenzoic acid with platinum doped TiO₂. *J. Hazard. Mater.* 167: 763–769.

- Sayan, E., Edecan, M.E. 2008. An optimization study using response surface methods on the decolorization of reactive blue 19 from aqueous solution by ultrasound. *Ultrason. Sonochem.* 15: 530–538.
- Shankar, M.V., Anandan, S., Venkatachalam, V., Arabindoo, B., Murugesan, V. 2006. Fine route for an efficient removal of 2,4-dichlorophenoxyacetic acid (2, 4-D) by zeolite-supported TiO₂. *Chemosphere* 63: 1014–1021.
- Slimena, H., Houas, A., Nogier, J.P. 2011. Elaboration of stable anatase TiO₂ through activated carbon addition with high photocatalytic activity under visible light. *J. Photochem. Photobiol. A: Chem.* 221: 13–21.
- Wang, X., Hu, Z., Chen, Y., Zhao, G., Liu, Y., Wen, Z. 2009. A novel approach towards high performance composite photocatalyst of TiO₂ deposited on activated carbon. *Appl. Surface Sci.* 255: 3953–3958.
- Wang, X., Liu, Y., Hu, Z., Chen, Y., Liu, W., Zhao, G. 2009. Degradation of methyl orange by composite photocatalysts nano-TiO₂ immobilized on activated carbons of different porosities. *J. Hazard. Mater.* 169: 1061–1067.
- Xiang, B., Zhang, Y., Wang, Z., Luo, X.H., Zhu, Y.W., Zhang, H.Z., Yu D.P. 2005. Field-emission properties of TiO₂ nanowire arrays. *J. Phys. D* 38: 1152–1155.
- Yazawa, T., Machida, F., Kubo, N., Jin, T. 2009. Photocatalytic activity of transparent porous glass supported TiO₂. *Ceram. Int.* 35: 3321–33258.
- Yu, Y., Yu, J.C., Yu, J.G., Kwok, Y.C., Che, Y.K., Zhao, J.C., Ding, L., Ge, W.K., Wong, P.K. 2005. Enhancement of photocatalytic activity of mesoporous TiO₂ by using carbon nanotube. *Appl. Catal. A: General* 289: 186–196.
- Zhang, H., Banfield, J.F. 2005. Size dependence of the kinetic rate constant for phase transformation in TiO₂ nanoparticles. *Chem. Mater.* 17: 3421–3425.
- Zhang, X., Zhou, M., Lei, L. 2005. Preparation of anatase TiO₂ supported on alumina by different metal organic chemical vapor deposition methods. *Appl. Catal. A: General* 282: 285–293.
- Zhao, W., Bai, Z., Ren, A., Guo, B., Wu, C. 2010. Sunlight photocatalytic activity of CdS modified TiO₂ loaded on activated carbon fibers. *Appl. Surface Sci.* 256: 3493–3498.
